

# Correlation lengths of flat-band superconductivity from quantum geometry

S. S. Elden and M. Iskin

*Department of Physics, Koç University, Rumelifeneri Yolu, 34450 Sarıyer, İstanbul, Türkiye*

(Dated: January 21, 2026)

Flat-band superconductors provide a regime in which kinetic energy is quenched, so that pairing is governed primarily by interactions and quantum geometry. We investigate characteristic superconducting length scales in all-flat-band systems under the assumptions of time-reversal symmetry and spatially-uniform pairing, focusing on the size of the lowest-lying two-body bound state, the average Cooper-pair size, and the zero-temperature coherence length in two-band Hubbard models. Using the Creutz ladder and the  $\chi$  lattice as representative examples, we show that both the two-body bound-state size and the many-body Cooper-pair size remain finite and small in the weak-coupling limit, being controlled by the quantum metric of the flat bands. By contrast, the coherence length exhibits qualitatively distinct behavior, diverging in the dilute limit and in the vicinity of insulating regimes. These results demonstrate that, in flat-band superconductors, the pair size and the coherence length are fundamentally distinct physical quantities and highlight the central role of band geometry in shaping superconducting length scales when kinetic energy is quenched.

## I. INTRODUCTION

Flat-band superconductivity represents a profound departure from conventional BCS theory, as pairing can emerge even in the complete absence of kinetic-energy dispersion, rendering interaction effects and the geometry of Bloch states central to the superconducting phenomenology [1–5]. Early studies established that flat bands can support superconductivity with a critical temperature that scales linearly with the interaction strength [6]; subsequent work has shown, however, that superconducting coherence is governed not by the density of states alone but by the quantum geometry of the underlying band structure [1–3]. In particular, the quantum metric tensor, which quantifies distances between Bloch states in momentum space, becomes especially relevant when band dispersion is quenched and conventional dispersion-based mechanisms for superconductivity are absent. Until very recently, the quantum metric could not be accessed experimentally in solid-state systems; however, two independent breakthroughs have now shown that quantum geometry is directly observable in crystalline materials, rather than only indirectly deduced [7–9].

In conventional superconductors with dispersive bands, characteristic length scales such as the Cooper-pair size and the coherence length are set by the band curvature and the pairing gap. Although these quantities are physically distinct, within weak-coupling BCS theory they scale identically and are controlled by the ratio of the Fermi velocity  $v_F$  to the superconducting gap  $\Delta_0$ , namely  $\xi_{\text{pair}} \sim \xi_{\text{BCS}} \sim \hbar v_F / \Delta_0$  in the BCS limit [10–12]. Since  $\Delta_0$  is exponentially small in this regime, the coherence length becomes very large and Cooper pairs strongly overlap. By contrast, in flat-band systems the Fermi velocity is ill defined due to the absence of band dispersion, and conventional BCS length scales consequently lose their meaning, motivating geometry-based characterizations of superconducting correlations [13].

Recently, several distinct superconducting length

scales have been investigated in flat-band systems [14–23]. For instance, it has been proposed that the coherence length  $\xi$  acquires an anomalous quantum-geometric contribution and can be expressed as  $\xi = \sqrt{\xi_{\text{BCS}}^2 + l_{\text{qm}}^2}$ , where  $l_{\text{qm}}$  is controlled by the quantum metric [15]. Within this picture,  $\xi$  remains finite in the flat-band limit and is bounded from below by  $l_{\text{qm}}$ . By contrast, an alternative approach based on extracting characteristic length scales from the spatial decay of correlation functions within real-space Bogoliubov-de Gennes frameworks [16] has reached the opposite conclusion, namely that  $\xi$  is disconnected from the quantum metric and exhibits no lower bound [24]. Furthermore, quantum-geometric effects on the Ginzburg-Landau coherence length, as well as on the sizes of two-body bound states and Cooper pairs, have been examined using BCS-BEC crossover and localization-tensor formalisms [17, 18]. These studies indicate that the various superconducting length scales depend on the quantum metric in more intricate and mutually distinct ways, suggesting that their relation to quantum geometry is not described by a single, unified behavior.

In this work, we analyze characteristic superconducting length scales in multiband systems with perfectly flat bands under the assumptions of uniform pairing and the presence of time-reversal and sublattice-exchange symmetries. Focusing on the size of the lowest-lying two-body bound state, the average Cooper-pair size within mean-field BCS-BEC crossover theory, and the zero-temperature coherence length obtained from Gaussian fluctuations, we show that the pair size remains finite and small in the weak-coupling limit and is governed by the quantum geometry of the Bloch states. By contrast, the coherence length exhibits qualitatively different behavior and diverges in the dilute and insulating limits. These results are consistent with and complementary to earlier studies emphasizing quantum-geometric contributions to superconducting coherence, while clarifying that pair size and coherence length are distinct physical quantities in

flat-band superconductors. More importantly, by explicitly analyzing the Creutz and  $\chi$  lattices considered in Ref. [16], our findings help reconcile recent disagreements regarding superconducting length scales in flat-band systems [15, 16, 18, 24].

The remainder of this paper is organized as follows. In Sec. II, we introduce the multiband Hubbard model in reciprocal space and define the characteristic superconducting length scales considered in this work. In Sec. III, we present numerical results for two representative all-flat-band lattices and discuss their implications in the context of the recent controversy. Finally, Sec. IV summarizes our main findings and conclusions.

## II. THEORETICAL FORMALISM

In our theoretical formulation, we start from a tight-binding Hubbard model defined on a lattice with a multi-orbital basis and transform it to reciprocal space. For simplicity, we assume time-reversal symmetry and spatially uniform pairing, and restrict our attention to two-band Hubbard models with perfectly flat bands. This setting allows us to cleanly isolate and analyze the impact of quantum geometry on the resulting characteristic length scales, free from conventional contributions associated with band dispersion.

### A. Multiband Hubbard Hamiltonian

In general, the multi-orbital Hubbard Hamiltonian can be written as

$$\mathcal{H} = \sum_{\sigma} \mathcal{H}_{\sigma} + \mathcal{H}_{\uparrow\downarrow}. \quad (1)$$

Here, the single-particle contribution  $\mathcal{H}_{\sigma} = -\sum_{i' S' S} t_{iS, i'S'}^{\sigma} c_{Si\sigma}^{\dagger} c_{S'i'\sigma}$  describes hopping between lattice sites, where  $c_{Si\sigma}^{\dagger}$  creates a particle with spin  $\sigma = \{\uparrow, \downarrow\}$  on the sublattice site  $S = \{A, B\}$  within the unit cell  $i$ , and  $t_{iS, i'S'}^{\sigma}$  denotes the hopping amplitude between sites  $S' \in i'$  and  $S \in i$ . We assume short-ranged interparticle interactions described by  $\mathcal{H}_{\uparrow\downarrow} = -U \sum_{iS} c_{iS\uparrow}^{\dagger} c_{iS\downarrow}^{\dagger} c_{iS\downarrow} c_{iS\uparrow}$ , which corresponds to a local attraction of strength  $U \geq 0$  between opposite-spin particles occupying the same site.

To transform the Hamiltonian to reciprocal space, we use the Fourier expansion  $c_{Si\sigma}^{\dagger} = \frac{1}{\sqrt{N_c}} \sum_{\mathbf{k}} e^{-i\mathbf{k} \cdot \mathbf{r}_{iS}} c_{S\mathbf{k}\sigma}^{\dagger}$ , where  $N_c$  is the number of unit cells,  $\mathbf{k}$  runs over the first Brillouin zone (BZ) satisfying  $\sum_{\mathbf{k} \in \text{BZ}} 1 = N_c$ , and  $\mathbf{r}_{iS}$  denotes the position of site  $S \in i$ . Since each unit cell contains two sublattice sites, the total number of lattice sites is  $N = 2N_c$ . Under this transformation, the non-interacting term becomes  $\mathcal{H}_{\sigma} = \sum_{\mathbf{k}} h_{SS'\mathbf{k}}^{\sigma} c_{S\mathbf{k}\sigma}^{\dagger} c_{S'\mathbf{k}\sigma}$ , where  $h_{SS'\mathbf{k}}^{\sigma} = -\frac{1}{N_c} \sum_{i' S' S} t_{iS, i'S'}^{\sigma} e^{i\mathbf{k} \cdot (\mathbf{r}_{iS} - \mathbf{r}_{i'S'})}$  defines the  $2 \times 2$  Bloch Hamiltonian in the sublattice basis. This

leads to the eigenvalue problem

$$\sum_{S'} h_{SS'\mathbf{k}}^{\sigma} n_{S'\mathbf{k}\sigma} = \epsilon_{n\mathbf{k}\sigma} n_{S\mathbf{k}\sigma}, \quad (2)$$

where  $\epsilon_{n\mathbf{k}\sigma}$  with  $n = \{1, 2\}$  is the energy of the  $n$ th Bloch band and  $n_{S\mathbf{k}\sigma} = \langle S | n_{\mathbf{k}\sigma} \rangle$  is the sublattice projection of the periodic part of the corresponding Bloch state  $|n_{\mathbf{k}\sigma}\rangle$ . Transforming further to the band basis,  $c_{n\mathbf{k}\sigma}^{\dagger} = \sum_S n_{S\mathbf{k}\sigma} c_{S\mathbf{k}\sigma}^{\dagger}$ , the non-interacting Hamiltonian takes the diagonal form

$$\mathcal{H}_{\sigma} = \sum_{n\mathbf{k}} \epsilon_{n\mathbf{k}\sigma} c_{n\mathbf{k}\sigma}^{\dagger} c_{n\mathbf{k}\sigma}. \quad (3)$$

We focus on systems with two perfectly flat bands that possess time-reversal and particle-hole symmetries, implying  $\epsilon_{n, -\mathbf{k}, \downarrow} = \epsilon_{n\mathbf{k}, \uparrow} \equiv \epsilon_n$ , with  $\epsilon_2 = -\epsilon_1 \equiv \epsilon$ , and  $n_{S, -\mathbf{k}, \downarrow}^* = n_{S\mathbf{k}, \uparrow} \equiv n_{S\mathbf{k}}$ .

In reciprocal space, the onsite multi-orbital Hubbard interaction becomes  $\mathcal{H}_{\uparrow\downarrow} = -\frac{U}{N_c} \sum_{S\mathbf{k}\mathbf{k}'\mathbf{q}} c_{S, \mathbf{k}+\frac{\mathbf{q}}{2}, \uparrow}^{\dagger} c_{S, -\mathbf{k}+\frac{\mathbf{q}}{2}, \downarrow}^{\dagger} c_{S, -\mathbf{k}+\frac{\mathbf{q}}{2}, \downarrow} c_{S, \mathbf{k}+\frac{\mathbf{q}}{2}, \uparrow}$ , and, upon transforming to the band basis, takes the form

$$\mathcal{H}_{\uparrow\downarrow} = \frac{1}{N_c} \sum_{\substack{n m m' m' \\ \mathbf{k} \mathbf{k}' \mathbf{q}}} U_{n m m' \mathbf{k}'}^{\text{nmk}}(\mathbf{q}) b_{nm}^{\dagger}(\mathbf{k}, \mathbf{q}) b_{n' m'}(\mathbf{k}', \mathbf{q}). \quad (4)$$

Here, the interaction matrix elements  $U_{n m m' \mathbf{k}'}^{\text{nmk}}(\mathbf{q}) = -U \sum_S n_{S, \mathbf{k}+\frac{\mathbf{q}}{2}, \uparrow}^* m_{S, -\mathbf{k}+\frac{\mathbf{q}}{2}, \downarrow}^* m_{S, -\mathbf{k}+\frac{\mathbf{q}}{2}, \downarrow}^* n_{S, \mathbf{k}+\frac{\mathbf{q}}{2}, \uparrow}^*$  are nontrivially dressed by the Bloch factors, and  $b_{nm}^{\dagger}(\mathbf{k}, \mathbf{q}) = c_{n, \mathbf{k}+\frac{\mathbf{q}}{2}, \uparrow}^{\dagger} c_{m, -\mathbf{k}+\frac{\mathbf{q}}{2}, \downarrow}^{\dagger}$  creates a pair of opposite-spin particles in bands  $n$  and  $m$  with relative momentum  $\mathbf{k}$  and total momentum  $\mathbf{q}$ . Equations (3) and (4) together provide an exact reciprocal-space representation of the multi-orbital Hubbard model, which we refer to as the multiband Hubbard model throughout this paper.

### B. Pair size for the two-body problem

To gain direct insight into the quantum-geometric origin of correlation lengths in flat-band superconductors, we first consider an exactly solvable two-body problem consisting of one spin- $\uparrow$  and one spin- $\downarrow$  particle on the lattice [25]. The bound states of this problem can be obtained exactly by employing the general ansatz  $|\Psi_{\mathbf{q}}\rangle = \sum_{nm\mathbf{k}} \alpha_{nm\mathbf{k}}^{\mathbf{q}} c_{n, \mathbf{k}+\frac{\mathbf{q}}{2}, \uparrow}^{\dagger} c_{m, -\mathbf{k}+\frac{\mathbf{q}}{2}, \downarrow}^{\dagger} |0\rangle$ , where  $|0\rangle$  denotes the vacuum state. Here,  $\mathbf{q}$  is the center-of-mass momentum of the spin-singlet pair, and the complex variational parameters satisfy the fermionic exchange symmetry  $\alpha_{nm\mathbf{k}}^{\mathbf{q}} = \alpha_{mn, -\mathbf{k}}^{\mathbf{q}}$ , together with the normalization condition  $\sum_{nm\mathbf{k}} |\alpha_{nm\mathbf{k}}^{\mathbf{q}}|^2 = 1$ . Spin-triplet bound states are excluded due to the onsite nature of the Hubbard interaction.

The energy  $E_{\mathbf{q}}$  of the two-body continuum and bound states is determined by minimizing  $\langle \Psi_{\mathbf{q}} | \mathcal{H} - E_{\mathbf{q}} | \Psi_{\mathbf{q}} \rangle$  with respect to  $\alpha_{nm\mathbf{k}}^{\mathbf{q}}$ , which leads to the linear equations  $(\epsilon_n + \epsilon_m - E_{\mathbf{q}}) \alpha_{nm\mathbf{k}}^{\mathbf{q}} = \frac{U}{N_c} \sum_S \beta_{S\mathbf{q}} n_{S,\mathbf{k}+\frac{\mathbf{q}}{2}}^* m_{S,\mathbf{k}-\frac{\mathbf{q}}{2}}$ . Here,  $E_{\mathbf{q}}$  plays the role of a Lagrange multiplier enforcing the normalization condition. Assuming time-reversal symmetry, we have introduced the dressed parameters  $\beta_{S\mathbf{q}} = \sum_{nm\mathbf{k}} \alpha_{nm\mathbf{k}}^{\mathbf{q}} n_{S,\mathbf{k}+\frac{\mathbf{q}}{2}}^* m_{S,\mathbf{k}-\frac{\mathbf{q}}{2}}$ , whose nonzero values serve as order parameters for the two-body bound states. For a given  $\mathbf{q}$ , the allowed values of  $E_{\mathbf{q}}$  can therefore be obtained by solving an eigenvalue problem of dimension  $4N_c \times 4N_c$ .

Alternatively, the bound-state energies can be determined from the nonlinear eigenvalue problem [25]  $\mathbf{G}^{\mathbf{q}} \boldsymbol{\beta}_{\mathbf{q}} = \mathbf{0}$ , where

$$G_{SS'}^{\mathbf{q}} = \delta_{SS'} - \frac{U}{N_c} \sum_{nm\mathbf{k}} \frac{n_{S,\mathbf{k}+\frac{\mathbf{q}}{2}}^* m_{S,\mathbf{k}-\frac{\mathbf{q}}{2}}^* n_{S',\mathbf{k}+\frac{\mathbf{q}}{2}}^* m_{S',\mathbf{k}-\frac{\mathbf{q}}{2}}^*}{\epsilon_n + \epsilon_m - E_{\mathbf{q}}} \quad (5)$$

is a  $2 \times 2$  Hermitian matrix. Here,  $\delta_{SS'}$  is the Kronecker delta, and nontrivial solutions for  $\boldsymbol{\beta}_{\mathbf{q}}$  correspond to values of  $E_{\mathbf{q}}$  at which  $\mathbf{G}_{\mathbf{q}}$  develops a zero eigenvalue. We focus on lattices that satisfy the uniform-pairing condition, namely that the eigenvector of  $\mathbf{G}_{\mathbf{q}}$  associated with the lowest-energy solution has equal weight on the two sublattices. In the  $\mathbf{q} \rightarrow \mathbf{0}$  limit, this implies  $\beta_{A\mathbf{q}} = \beta_{B\mathbf{q}} \equiv \beta_{\mathbf{q}}$ . We have verified numerically that this condition holds for the lowest-lying two-body bound states of the flat-band lattices considered in this work, where sublattice-exchange symmetry is present.

The size of a two-body bound state is characterized by the trace of the two-body localization tensor [18], whose matrix elements are defined as

$$(\xi_{2b}^2)_{ij} = \sum_{iS'i'S'} \bar{r}_i \bar{r}_j |\psi_{SS'}^{\mathbf{q}}(\bar{\mathbf{r}})|^2, \quad (6)$$

where  $\bar{r}_i$  ( $i = \{x, y, z\}$ ) denotes the components of the relative coordinate  $\bar{\mathbf{r}} = \mathbf{r}_{iS} - \mathbf{r}_{i'S'}$ , with  $\mathbf{r}_{iS}$  and  $\mathbf{r}_{i'S'}$  being the positions of the spin- $\uparrow$  and spin- $\downarrow$  particles, respectively. The relative wave function is given by  $\psi_{SS'}^{\mathbf{q}}(\bar{\mathbf{r}}) = \frac{1}{N_c} \sum_{nm\mathbf{k}} e^{i\mathbf{k} \cdot \bar{\mathbf{r}}} \alpha_{nm\mathbf{k}}^{\mathbf{q}} n_{S,\mathbf{k}+\frac{\mathbf{q}}{2}}^* m_{S',\mathbf{k}-\frac{\mathbf{q}}{2}}$ , up to an overall plane-wave factor associated with the center-of-mass motion. In the following, we restrict attention to the lowest two-body bound state at  $\mathbf{q} = \mathbf{0}$ , for which  $\alpha_{nm\mathbf{k}}^{\mathbf{0}} = \frac{U|\beta_{\mathbf{0}}|\delta_{nm}}{N_c(2\epsilon_n - E_b)}$  is independent of  $\mathbf{k}$ . The corresponding binding energy  $E_{\mathbf{0}} \equiv E_b$  is  $E_b = -\frac{U+\sqrt{U^2+16\epsilon^2}}{2}$ , which is valid for all  $U$  and follows from the condition  $\sum_{SS'} C_{SS'}^{\mathbf{0}} = 0$ , or equivalently,  $1 = \frac{U}{2} \sum_n \frac{1}{2\epsilon_n - E_b}$ , where we select the solution satisfying  $E_b \rightarrow -U$  in the strong-coupling limit  $U/t \gg 1$ .

Using integration by parts, the localization tensor can be expressed as  $(\xi_{2b}^2)_{ij} = \sum_{nmSS'\mathbf{k}} \alpha_{nm\mathbf{k}}^{\mathbf{0}} (\alpha_{nm\mathbf{k}}^{\mathbf{0}})^* \partial_{k_i} (n_{S\mathbf{k}} n_{S'\mathbf{k}}^*) \partial_{k_j} (m_{S\mathbf{k}}^* m_{S'\mathbf{k}})$ , which yields a purely interband contribution,

$(\xi_{2b}^2)_{ij} \equiv (\xi_{2b}^2)_{ij}^{\text{inter}}$ , with

$$(\xi_{2b}^2)_{ij}^{\text{inter}} = \frac{8\epsilon^2}{4\epsilon^2 + E_b^2} \frac{1}{N_c} \sum_{\mathbf{k}} g_{ij}^{\mathbf{k}}. \quad (7)$$

For the two-band models considered here, the quantum-metric tensors of the two flat bands are identical,  $g_{ij}^{1\mathbf{k}} = g_{ij}^{2\mathbf{k}} \equiv g_{ij}^{\mathbf{k}}$ , where

$$g_{ij}^{\mathbf{k}} = 2 \text{Re} \langle \partial_{k_i} 1_{\mathbf{k}} | 2_{\mathbf{k}} \rangle \langle 2_{\mathbf{k}} | \partial_{k_j} 1_{\mathbf{k}} \rangle. \quad (8)$$

More generally, the quantum-metric tensor of the  $n$ th Bloch band is  $g_{ij}^{n\mathbf{k}} = 2 \text{Re} \sum_{m \neq n} \langle \partial_{k_i} n_{\mathbf{k}} | m_{\mathbf{k}} \rangle \langle m_{\mathbf{k}} | \partial_{k_j} n_{\mathbf{k}} \rangle$ , which is, by construction, a real symmetric matrix [26, 27]. Consequently, the size of the lowest two-body bound state is entirely governed by the quantum metric of the flat bands. Importantly, Eq. (7) is exact for the  $\mathbf{q} = \mathbf{0}$  bound state for all values of  $U$ .

Finally, we note that the effective-mass tensor of the lowest two-body bound state can be extracted from Eq. (5) by expanding  $E_{\mathbf{q}} = E_b + \frac{1}{2} \sum_{ij} (M_{2b}^{-1})_{ij} q_i q_j + \dots$  in the  $\mathbf{q} \rightarrow \mathbf{0}$  limit where  $i = \{x, y, z\}$  [25]. This yields a purely interband contribution,  $(M_{2b}^{-1})_{ij} \equiv (M_{2b}^{-1})_{ij}^{\text{inter}}$ , with

$$(M_{2b}^{-1})_{ij}^{\text{inter}} = \frac{4\epsilon^2(4\epsilon^2 - E_b^2)}{E_b(4\epsilon^2 + E_b^2)} \frac{1}{N_c} \sum_{\mathbf{k}} g_{ij}^{\mathbf{k}}, \quad (9)$$

which is exact for the two-body problem. Note that  $(M_{2b}^{-1})_{ij} \rightarrow 0$  as  $E_b \rightarrow -2\epsilon$  when  $U = 0$ . This behavior originates from the perfectly flat single-particle bands, for which the constituent particle masses diverge, resulting in a divergent effective two-body mass. By contrast,  $(\xi_{2b}^2)_{ij} \rightarrow \frac{1}{N_c} \sum_{\mathbf{k}} g_{ij}^{\mathbf{k}}$  remains finite in the same limit, since it is controlled by the quantum geometry of the flat-band Bloch states rather than by band dispersion. Moreover, this expression provides the upper bound for the pair size. In dilute flat-band superconductors, the effective-mass tensor of Cooper pairs is well approximated by the same expression, with small corrections appearing at higher fillings [17]. We therefore employ Eq. (9) in Sec. III to analyze the coherence length in the many-body problem.

### C. Pair size for the many-body problem

We now turn to the average size of Cooper pairs within the mean-field BCS theory at zero temperature ( $T = 0$ ), under the same assumptions as in the two-body problem, namely time-reversal symmetry and the uniform-pairing condition [18]. Under these conditions, the onsite mean-field order parameter is independent of the sublattice and can be written as  $\Delta_A = \Delta_B \equiv \Delta_0$ , which can be chosen to be a positive real number without loss of generality. For the two-band Hubbard models with perfectly flat bands considered in this paper, the corresponding BCS ground state is  $|\text{BCS}\rangle = \prod_{n\mathbf{k}} (u_n + v_n c_{n\mathbf{k}\uparrow}^\dagger c_{n,-\mathbf{k}\downarrow}^\dagger) |0\rangle$ ,

where the coherence factors are  $u_n = \sqrt{\frac{1}{2} + \frac{\xi_n}{2E_n}}$ , and  $v_n = \sqrt{\frac{1}{2} - \frac{\xi_n}{2E_n}}$ . Here,  $\xi_n = \epsilon_n - \mu$  denotes the band energy measured from the chemical potential  $\mu$ , and  $E_n = \sqrt{\xi_n^2 + \Delta_0^2}$  is the quasiparticle spectrum. The parameters  $\Delta_0$  and  $\mu$  are determined self-consistently from the mean-field gap and number equations,

$$1 = \frac{U}{2} \sum_n \frac{1}{2E_n}, \quad (10)$$

$$F = 1 - \frac{1}{2} \sum_n \frac{\xi_n}{E_n}, \quad (11)$$

where the filling  $0 \leq F \leq 2$  denotes the total number of particles per lattice site. Equations (10) and (11) are well-established for providing a qualitatively accurate description of the BCS-BEC crossover physics at  $T = 0$  [28].

We define the properly normalized Cooper-pair wave function as [10, 18]

$$\Phi(\mathbf{r}_{iS}, \mathbf{r}_{i'S'}) = \frac{1}{A_{Cp}} \langle \text{BCS} | \psi_{\uparrow}^{\dagger}(\mathbf{r}_{iS}) \psi_{\downarrow}^{\dagger}(\mathbf{r}_{i'S'}) | \text{BCS} \rangle, \quad (12)$$

and expand the field operators in the Bloch basis,  $\psi_{\sigma}^{\dagger}(\mathbf{r}_{iS}) = \sum_{n\mathbf{k}} \phi_{n\mathbf{k}\sigma}^*(\mathbf{r}_{iS}) c_{n\mathbf{k}\sigma}^{\dagger}$ , where  $\phi_{n\mathbf{k}\sigma}(\mathbf{r}_{iS}) = \langle \mathbf{r}_{iS} | n\mathbf{k}\sigma \rangle = \frac{e^{i\mathbf{k}\cdot\mathbf{r}_{iS}}}{\sqrt{N_c}} n_{S\mathbf{k}\sigma}$  is the Bloch wave function. This yields  $\Phi(\mathbf{r}_{iS}, \mathbf{r}_{i'S'}) = \frac{1}{A_{Cp} N_c} \sum_{n\mathbf{k}} e^{-i\mathbf{k}\cdot\bar{\mathbf{r}}} u_n v_n n_{S\mathbf{k}}^* n_{S'\mathbf{k}}$ , where  $\bar{\mathbf{r}} = \mathbf{r}_{iS} - \mathbf{r}_{i'S'}$  is the relative coordinate. The normalization constant is  $A_{Cp} = \frac{N_c}{2} \sum_n \frac{\Delta_0^2}{2E_n^2}$ , which corresponds to the total number of condensed Cooper pairs [12].

In direct analogy with the two-body problem, the average size of Cooper pairs is characterized by the trace of the Cooper-pair localization tensor [18],

$$(\xi_{Cp}^2)_{ij} = \sum_{iSi'S'} \bar{r}_i \bar{r}_j |\Phi(\mathbf{r}_{iS}, \mathbf{r}_{i'S'})|^2. \quad (13)$$

Using integration by parts, this expression can be written as  $(\xi_{Cp}^2)_{ij} = \frac{1}{A_{Cp}} \sum_{nmSS'\mathbf{k}} u_n v_n u_m v_m \partial_{k_i} (n_{S\mathbf{k}} n_{S'\mathbf{k}}^*) \partial_{k_j} (m_{S\mathbf{k}}^* m_{S'\mathbf{k}})$ . For the flat-band models considered here, this reduces to a purely interband contribution,  $(\xi_{Cp}^2)_{ij} \equiv (\xi_{Cp}^2)_{ij}^{\text{inter}}$ , given by

$$(\xi_{Cp}^2)_{ij}^{\text{inter}} = \frac{(E_1 - E_2)^2}{E_1^2 + E_2^2} \frac{1}{N_c} \sum_{\mathbf{k}} g_{ij}^{\mathbf{k}}. \quad (14)$$

Thus, as in the two-body case, the average size of Cooper pairs is entirely governed by the quantum-metric tensor of the flat bands. Equation (14) is valid for all interaction strengths  $U$  and fillings  $F$  within the zero-temperature mean-field theory. Note that  $(\xi_{Cp}^2)_{ij} \rightarrow 0$  as  $E_1 \rightarrow E_2$ , i.e., at half filling with  $\mu = 0$  in particle-hole symmetric systems (provided that  $\Delta_0 \neq 0$ ), and at any filling in the  $U/t \rightarrow \infty$  limit.

#### D. Zero-temperature coherence length

To facilitate a direct comparison with the average size of Cooper pairs, we next introduce the zero-temperature coherence length for a multiband Hubbard model under the same assumptions of time-reversal symmetry and the uniform-pairing condition [17]. Unlike the Cooper-pair size, this is a beyond-mean-field quantity that is defined through the effective Gaussian action describing fluctuations of the superconducting order parameter about the mean-field saddle point. We assume that, in the long-wavelength limit  $Q \rightarrow 0$ , fluctuations of the order parameter remain uniform across the lattice. Accordingly, we introduce the Hubbard-Stratonovich field  $\Delta_{SQ} = \Delta_0 + \Lambda_Q$ , which is taken to be independent of the sublattice index, with  $\Lambda_{AQ} = \Lambda_{BQ} \equiv \Lambda_Q$  describing fluctuations around the saddle-point value  $\Delta_0$ . Here,  $Q \equiv (\mathbf{q}, i\nu_l)$  is a collective index, where  $\nu_l = 2\pi l T$  denotes the bosonic Matsubara frequency,  $T$  is the temperature, and  $l = 0, \pm 1, \pm 2, \dots$  is an integer. Throughout, we use units in which  $\hbar = 1$  and  $k_B = 1$ .

After a lengthy but straightforward calculation [17], the Gaussian action for the order-parameter fluctuations can be written as  $\mathcal{S}_G = \frac{N}{2T} \sum_Q (\Lambda_Q^* \Lambda_{-Q}) \mathcal{M}^Q \begin{pmatrix} \Lambda_Q \\ \Lambda_{-Q}^* \end{pmatrix}$ , where the fluctuation matrix  $\mathcal{M}^Q$  plays the role of the inverse propagator for amplitude and phase fluctuations. The zero-temperature coherence length is defined by setting  $i\nu_l = 0$  and focusing on the amplitude-amplitude sector in the long-wavelength limit [29, 30], specifically on the combination  $\mathcal{M}_{11}^{\mathbf{q}} + \mathcal{M}_{12}^{\mathbf{q}}$ . Expanding this quantity for  $\mathbf{q} \rightarrow \mathbf{0}$  yields  $\mathcal{M}_{11}^{\mathbf{q}} + \mathcal{M}_{12}^{\mathbf{q}} = A + \sum_{ij} C_{ij} q_i q_j$ , where  $A$  is the static coefficient and  $C_{ij} \equiv C_{ij}^{\text{inter}}$  is a purely interband kinetic coefficient. Explicitly, these coefficients are given by

$$A = \frac{\Delta_0^2}{4E_1^3} + \frac{\Delta_0^2}{4E_2^3}, \quad (15)$$

$$C_{ij}^{\text{inter}} = \left( \frac{\xi_1^2}{8E_1^3} + \frac{\xi_2^2}{8E_2^3} - \frac{\xi_1 \xi_2 + E_1 E_2 - \Delta_0^2}{4E_1 E_2 (E_1 + E_2)} \right) \frac{1}{N_c} \sum_{\mathbf{k}} g_{ij}^{\mathbf{k}}, \quad (16)$$

where the saddle-point parameters  $\Delta_0$  and  $\mu$  are determined self-consistently from Eqs. (10) and (11).

Provided that the trace of  $C_{ij}$  is positive, the zero-temperature coherence length is well defined and has a purely interband origin,  $(\xi_0^2)_{ij} \equiv (\xi_0^2)_{ij}^{\text{inter}}$ , characterized by [17]

$$(\xi_0^2)_{ij}^{\text{inter}} = \frac{C_{ij}^{\text{inter}}}{A}. \quad (17)$$

Thus, in direct analogy with  $(\xi_{2b}^2)_{ij}$  and  $(\xi_{Cp}^2)_{ij}$ , the zero-temperature coherence length is entirely governed by the quantum-metric tensor of the flat bands. It is also referred to as the Higgs-mode correlation length [22, 23]. While Eq. (17) formally applies for all interaction

strengths  $U$  and fillings  $F$  within the mean-field framework, our numerical analysis shows that the trace of  $C_{ij}$  may become negative near quarter filling. In this regime,  $(\xi_0^2)_{ij}$  ceases to be physical, as discussed in Sec. III. Similar to  $(\xi_{\text{CP}}^2)_{ij}$ , we also note that  $(\xi_0^2)_{ij} \rightarrow 0$  as  $E_1 \rightarrow E_2$  at any filling in the  $U/t \rightarrow \infty$  limit.

### III. NUMERICAL RESULTS AND DISCUSSION

In the previous section, we introduced the characteristic length scales of a two-band Hubbard model with perfectly flat bands, assuming time-reversal symmetry and a uniform-pairing condition. In this section, we demonstrate these results numerically by analyzing two representative lattice models: (i) the Creutz ladder and (ii) the  $\chi$  lattice, both of which are depicted in Fig. 1.

The Creutz ladder is a one-dimensional, two-legged lattice with two sublattices. It is described by the Bloch Hamiltonian  $h_{\downarrow, -k}^* = h_{\uparrow k} \equiv h_k$ , with [16]

$$h_k = \begin{bmatrix} -2t \sin(ka) & -2t \cos(ka) \\ -2t \cos(ka) & 2t \sin(ka) \end{bmatrix}. \quad (18)$$

Here,  $a$  is the lattice spacing, and  $-\pi/a \leq k < \pi/a$  defines the BZ. The Bloch spectrum consists of two perfectly flat bands,  $\epsilon_{2k} = -\epsilon_{1k} = 2t$ , and the associated Bloch states have sublattice components  $1_{Ak} = -2_{Bk} = \sin \gamma_k$  and  $1_{Bk} = 2_{Ak} = \cos \gamma_k$ , where  $\gamma_k = ka/2 + \pi/4$ . The quantum metric associated with these flat bands is momentum independent and takes the diagonal form  $g_{ij}^k = g_k \delta_{ij}$ , with  $g_k = a^2/2$ .

The  $\chi$  lattice is a two-dimensional square lattice with two sublattices, where the parameter  $\chi$  controls the strength of the long-range hopping process. It is described by the Bloch Hamiltonian  $h_{\downarrow, -\mathbf{k}}^* = h_{\uparrow \mathbf{k}} \equiv h_{\mathbf{k}}$ , with [16, 31, 32]

$$h_{\mathbf{k}} = \begin{bmatrix} 0 & -te^{-i\gamma_{\mathbf{k}}} \\ -te^{i\gamma_{\mathbf{k}}} & 0 \end{bmatrix}. \quad (19)$$

Here,  $a$  is the lattice spacing, and  $-\pi/a \leq k_x < \pi/a$  and  $-\pi/a \leq k_y < \pi/a$  define the BZ, with  $\gamma_{\mathbf{k}} = \chi [\cos(k_x a) + \cos(k_y a)]$ . Its Bloch spectrum again consists of two perfectly flat bands,  $\epsilon_{2\mathbf{k}} = -\epsilon_{1\mathbf{k}} = t$ , and the associated Bloch states have sublattice components  $1_{Ak} = 2_{Bk} = \frac{1}{\sqrt{2}}$  and  $1_{Bk} = -2_{Ak}^* = \frac{e^{i\gamma_{\mathbf{k}}}}{\sqrt{2}}$ . The quantum metric associated with these flat bands is  $g_{ij}^{\mathbf{k}} = \frac{a^2 \chi^2}{2} \sin(k_x a) \sin(k_y a)$ . In our numerical calculations, we set  $\chi = 1$ .

First, we note that both lattices possess not only time-reversal symmetry by construction but also sublattice-exchange and particle-hole symmetries. As a consequence of the former symmetry, Eq. (5) implies that  $G_{AA}^0 = G_{BB}^0$  and  $G_{AB}^0 = G_{BA}^0$  for the lowest bound ( $\mathbf{q} = \mathbf{0}$ ) two-body state. These relations imply that the vector  $\frac{1}{\sqrt{2}} (1 \ \pm 1)^T$ , with  $T$  denoting the transpose, is an

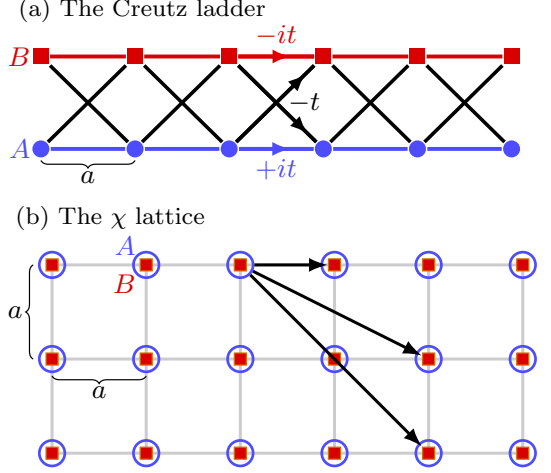


FIG. 1. Illustration of (a) the Creutz ladder and (b) the  $\chi$  lattice. Blue circles (A) and red squares (B) denote the two sublattices, and the lattice spacing is denoted by  $a$ . In the  $\chi$  lattice, each lattice site hosts two orbitals (A and B), and long-range hopping processes connect A and B orbitals on different lattice sites, as indicated by the arrows.

eigenvector corresponding to the eigenvalue  $G_{AA}^0 \pm G_{AB}^0$ , respectively. Thus, by setting the + eigenvalue to zero, we can determine the binding energy  $E_b$  of the lowest bound two-body state. This result demonstrates that the uniform-pairing condition, i.e., the + eigenvector, is satisfied exactly for the two-body problem in both lattices, and therefore that the analyses of the previous sections are applicable. We have also numerically verified this observation, finding that  $\beta_{A\mathbf{q}} = \beta_{B\mathbf{q}}$  holds with numerical exactness as  $\mathbf{q} \rightarrow \mathbf{0}$ . Furthermore, the uniform-pairing condition is known to be satisfied for the many-body problem in both lattices within the real-space Bogoliubov-de Gennes formulation of the mean-field theory [16]. See also Ref. [33].

In Fig. 2, we present the self-consistent solutions of Eqs. (10) and (11) for the mean-field parameters  $\Delta_0$  and  $\mu$ . Owing to particle-hole symmetry, all results are symmetric about half filling ( $F = 1$ ), and we therefore present them only in the range  $0 \leq F \leq 1$ . For instance, in the  $U/t \rightarrow 0$  limit, our numerical solutions are fully consistent with the analytical expectations that  $\mu = -\epsilon - \frac{U}{4}(1 - 2F)$  and  $\Delta_0 = \frac{U}{2}\sqrt{F(1 - F)}$  for  $0 \leq F < 1$ , and  $\mu = \epsilon - \frac{U}{4}(3 - 2F)$  and  $\Delta_0 = \frac{U}{2}\sqrt{(F - 1)(2 - F)}$  for  $1 < F \leq 2$ . Note that  $(-\mu, \Delta_0)$  are solutions of Eqs. (10) and (11) for  $U$  and  $2 - F$ , provided that  $(\mu, \Delta_0)$  are solutions for given  $U$  and  $F$ . In addition, we verified that  $\mu = -\frac{U}{2}(1 - F)$  and  $\Delta_0 = \frac{U}{2}\sqrt{F(2 - F)}$  in the  $U/t \rightarrow \infty$  limit.

The simplicity of the Bloch spectrum further allows an analytic solution of the mean-field equations at half filling, for which we find  $\mu = \pm\sqrt{\epsilon^2 - U\epsilon/2}$  together with

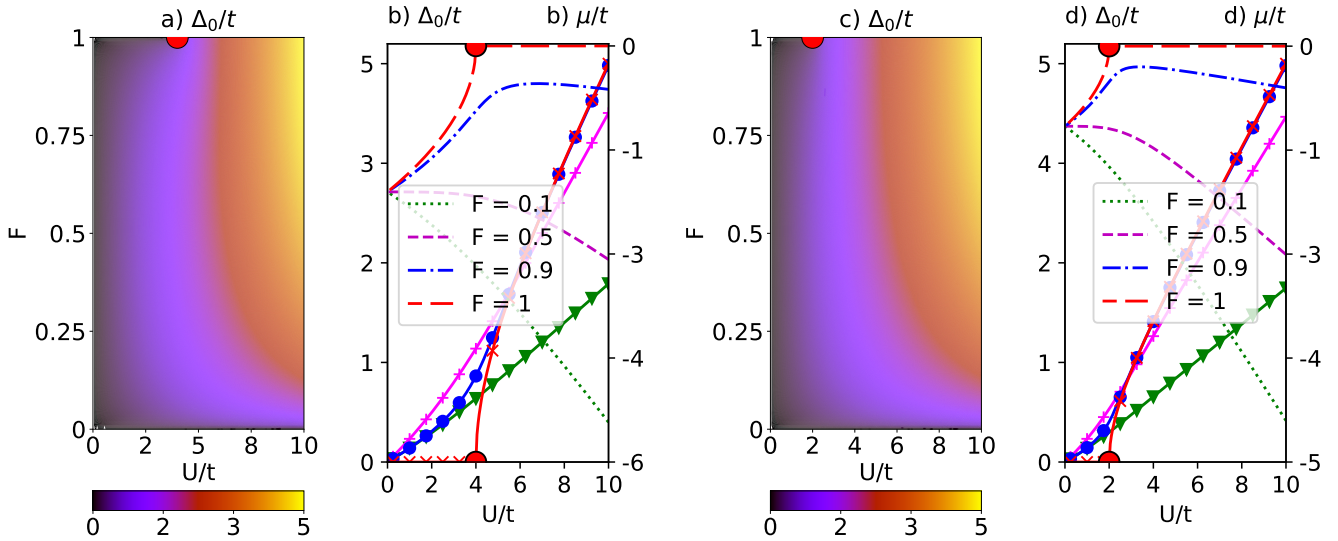


FIG. 2. The order parameter  $\Delta_0$  is shown in (a) for the Creutz ladder and in (c) for the  $\chi$  lattice as functions of the particle filling  $F$  and the interaction strength  $U$ . The corresponding line cuts are shown in (b) for the Creutz ladder and in (d) for the  $\chi$  lattice, where  $\Delta_0$  is plotted with solid lines and markers, and the chemical potential  $\mu$  is shown with dashed lines. At half filling ( $F = 1$ ),  $\Delta_0$  vanishes and  $\mu$  is pinned within a finite interval, signaling an insulating state, for interaction strengths below a critical threshold  $U < U_c$ . The red dots mark the location of  $U_c = 2\epsilon$ .

$\Delta_0 = 0$  when  $U \leq U_c = 2\epsilon$ , and  $\mu = 0$  together with  $\Delta_0 = \sqrt{U^2/4 - \epsilon^2}$  when  $U \geq U_c$ . These results are also visible in Fig. 2(b) for the Creutz ladder and Fig. 2(d) for the  $\chi$  lattice. The critical interaction threshold is given by the band gap, i.e.,  $U_c = 2\epsilon$ , and it is marked by a red dot in all panels. At half filling, when  $U < U_c$ , the vanishing  $\Delta_0$  indicates that the system remains in the normal state, while the pinning of  $\mu$  over a finite interval signals an insulating phase. The  $\pm$  signs in  $\mu$  correspond to particle- and hole-like excitations from the band insulator, respectively, and together they form an insulating dome in the figures. Previous DMRG and mean-field studies [33] of the Creutz ladder have already identified the half-filled system as a band insulator, and our analysis suggests that this insulating state persists up to  $U_c = 2\epsilon$  within the mean-field approximation. For interactions  $U > U_c$ , the system transitions to a superconducting phase, which can account for the finite superfluid weight reported in mean-field calculations at  $U = 8t$  [33]. In the remainder of this discussion, we exclude the parameter regime in which  $\Delta_0$  vanishes, since the length scales introduced in Sec. II require a nonzero  $\Delta_0$  to begin with.

In Fig. 3, we present the self-consistent solution for the average Cooper-pair size obtained from Eq. (14) for the many-body problem, together with Eqs. (10) and (11), as well as the corresponding result from Eq. (7) for the two-body problem. We first note that the tensors are diagonal, i.e.,  $(\xi_{2b}^2)_{ij} = \xi_{2b}^2 \delta_{ij}$  and  $(\xi_{\text{CP}}^2)_{ij} = \xi_{\text{CP}}^2 \delta_{ij}$ , and isotropic as a direct consequence of the uniform-pairing condition.

In the dilute limit  $F \rightarrow 0$ , our numerical solutions are

fully consistent with the physically intuitive expectation that  $\xi_{\text{CP}} \rightarrow \xi_{2b}$  for all values of  $U/t$  [18]. This coincidence can also be obtained analytically from Eqs. (7) and (14) by noting that  $E_n \approx \xi_n$  and  $\mu \rightarrow E_b/2$  in the  $F \rightarrow 0$  limit. Similarly, in the  $U/t \rightarrow 0$  limit, we observe that  $\xi_{\text{CP}} \rightarrow \xi_{2b}$  for all values of  $F$ . This behavior can again be understood analytically by noting that  $E_b \rightarrow -2\epsilon$  and  $E_n \approx \xi_n \ll t$ , which leads to  $\{\xi_{2b}^2, \xi_{\text{CP}}^2\} \rightarrow \frac{1}{N_c} \sum_{\mathbf{k}} g_{\mathbf{k}}$  in the  $U/t \rightarrow 0$  limit. Thus, we expect  $\{\xi_{\text{CP}}^2, \xi_{2b}^2\} \rightarrow a^2/2$  for the Creutz ladder and  $\{\xi_{\text{CP}}^2, \xi_{2b}^2\} \rightarrow a^2 \chi^2/4$  for the  $\chi$  lattice, both of which are in excellent agreement with the numerical results.

More interestingly, our numerical results show that  $\xi_{\text{CP}}$  vanishes at half filling for all  $U > U_c$ , suggesting purely onsite Cooper pairs even in the  $\Delta_0/t \rightarrow 0$  limit. Whether this intriguing behavior is physical or an artifact of the present approximations requires further investigation. Thus, except at half filling, Cooper pairs generally have a finite and small size. This behavior contrasts sharply with that of conventional BCS superconductors, where the pair size scales inversely with  $\Delta_0$  and therefore diverges in the  $U/t \rightarrow 0$  limit. The absence of such a divergence here demonstrates that pairing in flat-band lattices is governed entirely by quantum geometry.

In Fig. 4, we present the self-consistent solution of the zero-temperature coherence length obtained from Eq. (17), together with Eqs. (10) and (11). Similar to the pair-size tensors, this tensor is also diagonal and isotropic,  $(\xi_0^2)_{ij} = \xi_0^2 \delta_{ij}$ , as a direct consequence of the uniform-pairing condition. The white regions in Figs. 4(a) and 4(c) correspond to parameter regimes

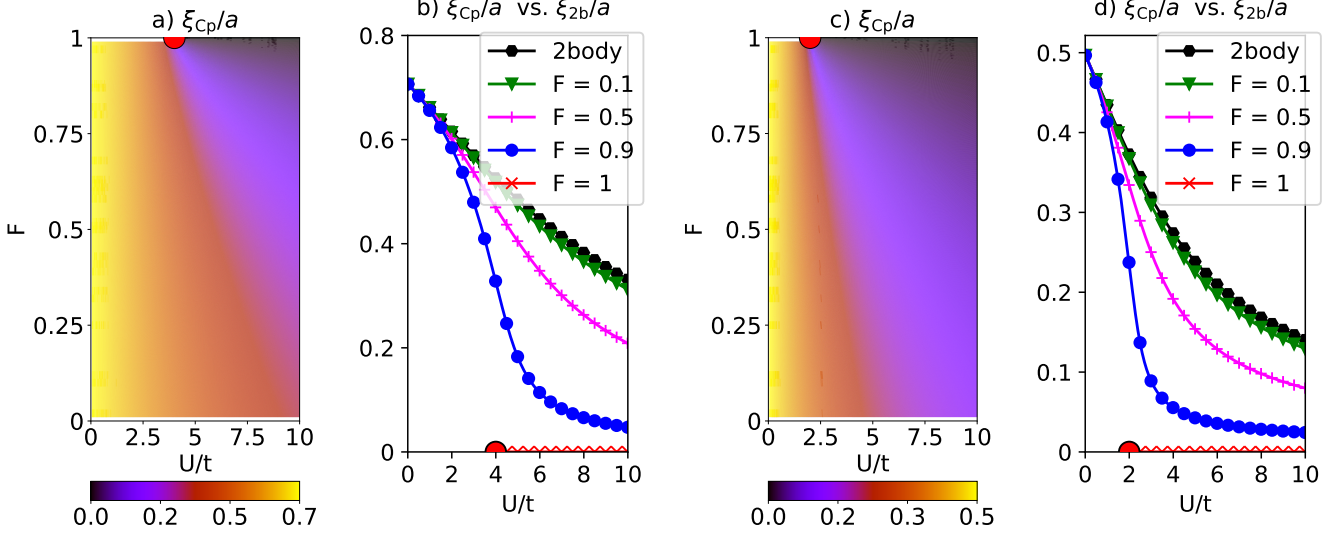


FIG. 3. The average Cooper-pair size  $\xi_{\text{Cp}}$  is shown in (a) for the Creutz ladder and in (c) for the  $\chi$  lattice as functions of the particle filling  $F$  and the interaction strength  $U$ . In panels (b) and (d), we compare  $\xi_{\text{Cp}}$  with the size of the lowest-bound two-body state  $\xi_{2b}$  for the Creutz ladder and the  $\chi$  lattice, respectively. Note that  $\xi_{\text{Cp}}$  reduces to  $\xi_{2b}$  in the dilute limit for all  $U$ . Parameter regimes in which  $\Delta_0 = 0$  are omitted.

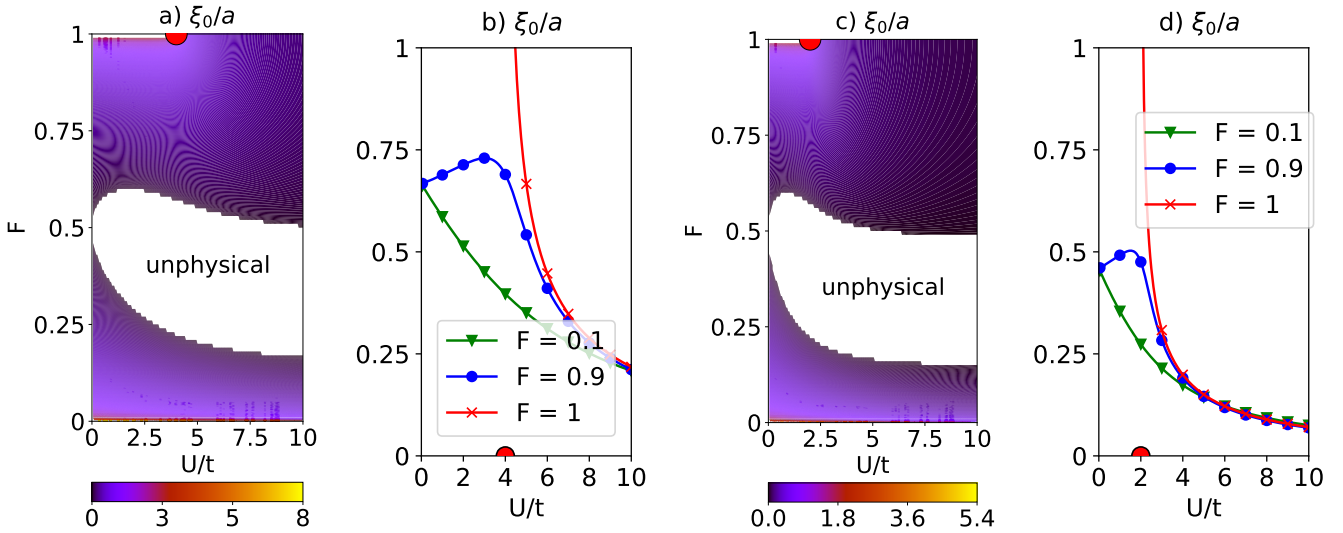


FIG. 4. The zero-temperature coherence length  $\xi_0$  is shown in (a) for the Creutz ladder and in (c) for the  $\chi$  lattice as functions of the particle filling  $F$  and the interaction strength  $U$ . Regions where  $\xi_0^2 < 0$  are shown in white, indicating that the coherence length is ill defined. In panels (b) and (d), we show representative line cuts for the Creutz ladder and the  $\chi$  lattice, respectively. The coherence length  $\xi_0$  diverges both in the dilute limit and in the vicinity of the insulating regime at half filling.

in which  $\xi_0^2$  becomes negative, rendering the coherence length ill defined. This issue can be cured by treating density fluctuations on the same footing as pairing fluctuations and subsequently performing the low- $\mathbf{q}$  expansion around the new minimum, where the amplitude-amplitude fluctuation sector occurs at a finite  $\mathbf{q} \neq \mathbf{0}$ , rather than at  $\mathbf{q} = \mathbf{0}$  [30]. Apart from this known subtlety, in the  $U/t \rightarrow 0$  limit our numerical calculations are fully consistent with the analytical expecta-

tion that  $(\xi_0^2)_{ij} \rightarrow \left[ \frac{1}{F(1-F)} - 4 \right] \frac{1}{8N_c} \sum_{\mathbf{k}} g_{ij}^{\mathbf{k}}$ . For instance, in the dilute limit  $F \rightarrow 0$ , the coherence length diverges as  $\xi_0^2 \rightarrow a^2/(16F)$  for the Creutz ladder and as  $\xi_0^2 \rightarrow a^2 \chi^2/(32F)$  for the  $\chi$  lattice.

To gain further insight into the physical origin of this divergence, we recast  $\xi_0$  in terms of effective pair parameters. We first note that the effective-mass tensor of the Cooper pairs,  $(M_{\text{Cp}}^{-1})_{ij}$ , approaches that of the lowest-

bound two-body states not only in the dilute regime but also at higher fillings, i.e.,  $(M_{\text{Cp}}^{-1})_{ij} \rightarrow (M_{2b}^{-1})_{ij}$ . This tensor is also diagonal and isotropic due to the uniform-pairing condition. For example, in the dilute limit when  $U/t \rightarrow 0$ , substituting  $E_b = -2\epsilon - U/2$  in Eq. (9) gives  $(M_{2b}^{-1})_{ij} = \frac{U}{2N_c} \sum_{\mathbf{k}} g_{ij}^{\mathbf{k}}$ , and we obtain

$$(\xi_0^2)_{ij} = \frac{(M_{\text{Cp}}^{-1})_{ij}}{4U_{\text{Cp}}F_{\text{Cp}}}, \quad (20)$$

where  $U_{\text{Cp}} = 2U$  is the effective onsite pair-pair repulsion and  $F_{\text{Cp}} = F/2$  denotes the effective pair filling, corresponding to the average number of condensed Cooper pairs per lattice site [17, 34]. Similarly, in the  $U/t \rightarrow \infty$  limit, we have  $E_b \rightarrow -U$ , which leads to  $(M_{\text{Cp}}^{-1})_{ij} = \frac{4\epsilon^2}{UN_c} \sum_{\mathbf{k}} g_{ij}^{\mathbf{k}}$ , together with  $A = F(2 - F)/U \rightarrow 2F/U$  and  $C_{ij} = \frac{2\epsilon^2}{U^3 N_c^2} \sum_{\mathbf{k}} g_{ij}^{\mathbf{k}}$ . This correspondence again reproduces essentially the correct bosonic form of the coherence length,  $(\xi_B^2)_{ij} = (M_B^{-1})_{ij}/(2U_{\text{BB}}F_B)$ , as expected for a weakly interacting dilute Bose gas, up to a numerical factor of order unity [17, 29, 30]. Thus, although  $\xi_0$  becomes unphysical near half filling, it correctly reproduces the coherence length in the dilute limit [35].

Furthermore, our numerical results demonstrate that  $\xi_0$  and  $\xi_{\text{Cp}}$  are generally of the same order of magnitude, except in the dilute limit and near half-filling as  $U \rightarrow U_c$ . Specifically,  $\xi_0$  diverges in the dilute limit for any  $U$ , as well as at half-filling ( $F = 1$ ) as  $U$  approaches  $U_c$ . This divergence highlights that  $\xi_0$  and  $\xi_{\text{Cp}}$  represent two distinct physical length scales, despite their close correspondence over a broad range of parameters. Although these quantities are physically distinct, they scale identically within weak-coupling BCS theory, where both are governed by the ratio of the Fermi velocity to the superconducting gap  $\Delta_0$ . Consequently, both length scales diverge in the  $U/t \rightarrow 0$  limit as  $\Delta_0 \rightarrow 0$ .

Our result on the absence of a BCS-like divergence of characteristic length scales in flat-band superconductors is consistent with the recent literature, where the pair size is characterized through the spatial decay of normal and anomalous correlation functions in real space [16]. In particular, for the Creutz ladder at quarter filling, the anomalous correlation function is shown to be strictly finite ranged, with no characteristic length scale exceeding the lattice spacing. For the  $\chi$  lattice, the anomalous correlation function is found to be strictly local, implying a vanishing Cooper-pair size. At first sight, these results appear to contradict our findings. However, this apparent discrepancy originates from the use of different, though closely related, definitions of the pair size.

To make this connection explicit, let's consider the anomalous correlation function  $K_{SS'}(\bar{\mathbf{r}}) = \langle c_{S\uparrow} c_{S'\downarrow} \rangle$  [16, 24]. By transforming this expression first to reciprocal space and then to the band basis, and by comparing the resulting expression with Eq. (12), one finds  $K_{SS'}(\bar{\mathbf{r}}) = -A_{\text{Cp}} \Phi^*(r_{iS}, r_{i'S'})$ . Consequently, the

Cooper-pair localization tensor can be reexpressed as

$$(\xi_{\text{Cp}}^2)_{ij} = \frac{\sum_{iSi'S'} \bar{r}_i \bar{r}_j |K_{SS'}(\bar{\mathbf{r}})|^2}{\sum_{iSi'S'} |K_{SS'}(\bar{\mathbf{r}})|^2}. \quad (21)$$

In the  $U/t \rightarrow 0$  limit at quarter filling, one finds  $K_{AA}(\bar{\mathbf{r}}) = K_{BB}(\bar{\mathbf{r}}) = (2\delta_{\bar{\mathbf{r}},0} - i\delta_{\bar{\mathbf{r}},a} + i\delta_{\bar{\mathbf{r}},-a})/8$  and  $K_{AB}(\bar{\mathbf{r}}) = K_{BA}(\bar{\mathbf{r}}) = (\delta_{\bar{\mathbf{r}},a} + \delta_{\bar{\mathbf{r}},-a})/8$  for the Creutz ladder [16]. Similarly, the anomalous correlators are given by  $K_{AA}(\bar{\mathbf{r}}) = K_{BB}(\bar{\mathbf{r}}) = \delta_{\bar{\mathbf{r}},0}/4$  and  $K_{AB}(\bar{\mathbf{r}}) = K_{BA}(\bar{\mathbf{r}}) = \frac{1}{4N_c} \sum_{\mathbf{k}} e^{i\bar{\mathbf{k}} \cdot \bar{\mathbf{r}}} e^{-i\gamma_{\mathbf{k}}}$  for the  $\chi$  lattice [16]. Substituting these expressions into Eq. (21) yields  $\xi_{\text{Cp}} = a/\sqrt{2}$  for the Creutz ladder and  $\xi_{\text{Cp}} = a\chi/2$  for the  $\chi$  lattice. These results are in perfect agreement with our analytical predictions and numerical calculations, thereby demonstrating the consistency between the correlation-function-based definition of the pair size obtained from the real-space Bogoliubov-de Gennes formalism and the geometry-based momentum-space formulation employed in this work.

Furthermore, according to Ref. [15], when all bands in the Bloch spectrum are perfectly flat, the coherence length is predicted to be a constant determined by a weighted average of the quantum metric. In sharp contrast, we find that neither the coherence length nor the pair size remains constant across parameter space. The only exception occurs at half filling, where the pair size vanishes, signaling strictly local pairing. In the strong-coupling limit  $U/t \rightarrow \infty$ , we further observe that the two-body pair size, the average Cooper-pair size, and the zero-temperature coherence length all scale inversely with  $U$ , in agreement with standard BCS-BEC crossover physics. This behavior demonstrates that, within our formulation, these characteristic length scales are not bounded from below, in contrast to the quantum-metric lower bound proposed in Ref. [15]. We attribute the origin of this discrepancy to the projection of fermionic operators onto the flat band employed in Ref. [15], which effectively restricts the analysis to the  $U/t \rightarrow 0$  limit. Within this restricted framework, the quantity identified as a lower bound in Ref. [15] instead emerges as an upper bound once interaction effects beyond the flat-band projection are properly taken into account. In the present work, we focus exclusively on all-flat two-band lattices in order to provide a transparent analysis and directly address the recent controversy raised in Refs. [16, 24]. Extensions to more general band structures, including systems with dispersive bands and with or without band touchings, are discussed in Refs. [14, 17, 18].

#### IV. CONCLUSION

In summary, we systematically examined characteristic length scales associated with pairing and coherence in superconducting systems with perfectly flat bands from three complementary perspectives. First, we analyzed the localization tensor of the lowest-lying two-body bound state. Second, we studied the average size

of Cooper pairs within the mean-field approximation. Third, we investigated the zero-temperature coherence length within the Gaussian-fluctuation theory. The presence of time-reversal and sublattice-exchange symmetries, which enforce spatially-uniform pairing, allowed us to substantially simplify the analysis and to cleanly isolate effects arising purely from quantum geometry.

Our results demonstrate that, throughout the parameter space, both the two-body pair size and the many-body Cooper-pair size, unlike in conventional superconductors with dispersive bands, do not exhibit a BCS-like divergence in the weak-coupling limit. Instead, these length scales remain finite and small, and are entirely governed by the quantum geometry of the underlying Bloch states. In particular, in the weak-coupling regime both pair sizes reduce to Brillouin-zone averages of the quantum metric, highlighting the central role of band geometry when kinetic energy is quenched.

The zero-temperature coherence length displays a related geometric origin, except in the dilute regime and in parameter regions that are insulating or proximate to an insulating phase, where its behavior becomes qualitatively distinct. This contrast highlights that the coherence length and the pair size encode fundamentally different physical information: while the pair size reflects

the internal spatial structure of bound fermion pairs, the coherence length is governed by collective properties and critical fluctuations of the superconducting state [34]. Taken together, our findings clarify the geometric origin of pairing length scales in flat-band superconductors and underscore the necessity of distinguishing between pair size and coherence length in such systems. Furthermore, we hope that this work helps clarify recent discussions concerning superconducting length scales in flat-band systems [15, 16, 18, 24].

Looking ahead, it would be valuable to explore how the geometric control of pairing length scales identified here evolves in more general settings, including weakly dispersive bands, multiband systems without sublattice-exchange symmetry, and treatments that incorporate beyond-mean-field corrections.

## ACKNOWLEDGMENTS

We acknowledge support from the U.S. Air Force Office of Scientific Research (AFOSR) under Grant No. FA8655-24-1-7391.

---

[1] P. Törmä, S. Peotta, and B. A. Bernevig, Superconductivity, superfluidity and quantum geometry in twisted multilayer systems, *Nature Reviews Physics* **4**, 528 (2022).

[2] S. Peotta, K.-E. Huhtinen, and P. Törmä, Quantum geometry in superfluidity and superconductivity, in *Proceedings of the International School of Physics “Enrico Fermi”, Course 211: Quantum Mixtures with Ultra-Cold Atoms*, Proceedings of the International School of Physics “Enrico Fermi”, Vol. 211, edited by R. Grimm, M. Inguscio, S. Stringari, and G. Lamporesi (IOS Press, 2025) pp. 373–404.

[3] J. Yu, B. A. Bernevig, R. Queiroz, E. Rossi, P. Törmä, and B.-J. Yang, Quantum geometry in quantum materials, *npj Quantum Materials* **10**, 101 (2025).

[4] T. Liu, X.-B. Qiang, H.-Z. Lu, and X. Xie, Quantum geometry in condensed matter, *National Science Review* **12**, nwae334 (2025).

[5] A. Gao, N. Nagaosa, N. Ni, and S.-Y. Xu, Quantum geometry phenomena in condensed matter systems, arXiv preprint arXiv:2508.00469 (2025).

[6] N. B. Kopnin, T. T. Heikkilä, and G. E. Volovik, High-temperature surface superconductivity in topological flat-band systems, *Phys. Rev. B* **83**, 220503 (2011).

[7] S. Kim, Y. Chung, Y. Qian, S. Park, C. Jozwiak, E. Rotenberg, A. Bostwick, K. S. Kim, and B.-J. Yang, Direct measurement of the quantum metric tensor in solids, *Science* **388**, 1050 (2025).

[8] M. Kang, S. Kim, Y. Qian, P. M. Neves, L. Ye, J. Jung, D. Puntel, F. Mazzola, S. Fang, C. Jozwiak, *et al.*, Measurements of the quantum geometric tensor in solids, *Nature Physics* **21**, 110 (2025).

[9] Y. Bohm-Jung, From Berry curvature to quantum metric: a new era of quantum geometry metrology for Bloch electrons in solids, *Chin. Phys. Lett.* (2026).

[10] P.-G. de Gennes, *Superconductivity of Metals and Alloys* (W.A. Benjamin, Inc., New York, 1966) chapter 4.

[11] J. F. Annett, *Superconductivity, superfluids and condensates*, Vol. 5 (Oxford University Press, 2004).

[12] A. J. Leggett, *Quantum Liquids: Bose Condensation and Cooper Pairing in Condensed-Matter Systems* (Oxford University Press, Oxford, UK, 2006).

[13] H. Tian, X. Gao, Y. Zhang, S. Che, T. Xu, P. Cheung, K. Watanabe, T. Taniguchi, M. Randeria, F. Zhang, *et al.*, Evidence for Dirac flat band superconductivity enabled by quantum geometry, *Nature* **614**, 440 (2023).

[14] M. Iskin, Extracting quantum-geometric effects from Ginzburg-Landau theory in a multiband Hubbard model, *Phys. Rev. B* **107**, 224505 (2023).

[15] J.-X. Hu, S. A. Chen, and K. T. Law, Anomalous coherence length in superconductors with quantum metric, *Communications Physics* **8**, 20 (2025).

[16] M. Thumin and G. Bouzerar, Correlation functions and characteristic lengthscales in flat band superconductors, *SciPost Physics* **18**, 025 (2025).

[17] M. Iskin, Coherence length and quantum geometry in a dilute flat-band superconductor, *Phys. Rev. B* **110**, 144505 (2024).

[18] M. Iskin, Pair size and quantum geometry in a multiband Hubbard model, *Physical Review B* **111**, 014502 (2025).

[19] C. Li, F.-C. Zhang, and L.-H. Hu, Vortex states and coherence lengths in flat-band superconductors, arXiv preprint arXiv:2505.01682 (2025).

[20] P. Virtanen, R. P. S. Penttilä, P. Törmä, A. Díez-Carlón,

D. K. Efetov, and T. T. Heikkilä, Superconducting junctions with flat bands, *Phys. Rev. B* **112**, L100502 (2025).

[21] S. Lee, S. H. Lee, and B.-J. Yang, Embedding independent length scale of flat bands, arXiv preprint arXiv:2511.02240 (2025).

[22] Y. Xiao and N. Hao, Effects of quantum geometry on the Higgs mode in flat-band superconductors, *Phys. Rev. B* **111**, 134502 (2025).

[23] C.-g. Oh, H. Watanabe, and N. Tsuji, Role of quantum geometry in the competition between Higgs mode and quasiparticles in third-harmonic generation of superconductors, arXiv preprint arXiv:2512.01200 (2025).

[24] See the referee reports in the submission and refereeing history of Ref. [16] for additional context on recent discussions concerning superconducting length scales in flat-band superconductors, in particular the reports by S. Peotta.

[25] M. Iskin, Two-body problem in a multiband lattice and the role of quantum geometry, *Phys. Rev. A* **103**, 053311 (2021).

[26] J. P. Provost and G. Vallee, Riemannian structure on manifolds of quantum states, *Commun. Math. Phys.* **76**, 289 (1980).

[27] R. Resta, The insulating state of matter: a geometrical theory, *The European Physical Journal B* **79**, 121 (2011).

[28] G. C. Strinati, P. Pieri, G. Röpke, P. Schuck, and M. Urban, The BCS-BEC crossover: From ultra-cold Fermi gases to nuclear systems, *Physics Reports* **738**, 1 (2018).

[29] F. Pistolesi and G. C. Strinati, Evolution from BCS superconductivity to Bose condensation: Calculation of the zero-temperature phase coherence length, *Phys. Rev. B* **53**, 15168 (1996).

[30] L. Benfatto, A. Toschi, S. Caprara, and C. Castellani, Coherence length in superconductors from weak to strong coupling, *Phys. Rev. B* **66**, 054515 (2002).

[31] J. S. Hofmann, D. Chowdhury, S. A. Kivelson, and E. Berg, Heuristic bounds on superconductivity and how to exceed them, *npj quantum materials* **7**, 83 (2022).

[32] J. S. Hofmann, E. Berg, and D. Chowdhury, Superconductivity, charge density wave, and supersolidity in flat bands with a tunable quantum metric, *Phys. Rev. Lett.* **130**, 226001 (2023).

[33] S. M. Chan, B. Grémaud, and G. G. Batrouni, Pairing and superconductivity in quasi-one-dimensional flat-band systems: Creutz and sawtooth lattices, *Phys. Rev. B* **105**, 024502 (2022).

[34] M. Iskin, Cooper pairing, flat-band superconductivity, and quantum geometry in the pyrochlore-Hubbard model, *Phys. Rev. B* **109**, 174508 (2024).

[35] Away from the dilute limit, in the  $U/t \rightarrow 0$  limit, the average number of condensed Cooper pairs per lattice site can be written as  $F(1-F)/2$ . One may therefore expect the relevant physical length scale to take the form  $(\xi_0^2)_{ij} \rightarrow \frac{1}{8F(1-F)N_c} \sum_k g_{ij}^k$ , in accordance with the bosonic expression for the coherence length.